Article

Cell Reports

# The Tumor Suppressor MIG6 Controls Mitotic Progression and the G2/M DNA Damage Checkpoint by Stabilizing the WEE1 Kinase

## Graphical Abstract

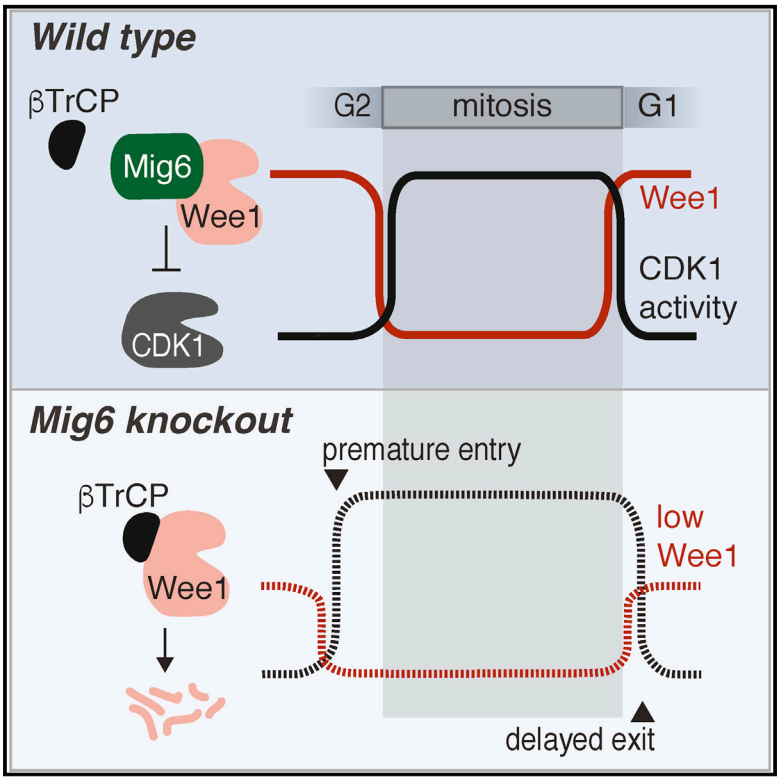


## Authors

Mari Sasaki, Takeshi Terabayashi, Stefanie M. Weiss, Ingvar Ferby

## Correspondence

ingvar.ferby@imbim.uu.se

## In Brief

Mig6 is a crucial tumor suppressor and negative regulator of EGFR (epidermal growth factor receptor). Sasaki et al. show that Mig6 also regulates cell cycle progression and promotes DNA-damage-induced cell cycle arrest by protecting Wee1, the inhibitory kinase of CDK1, from βTrCP-dependent proteasomal degradation.

## Highlights

- The EGFR inhibitor Mig6 controls progression through mitosis, independently of EGFR
- Mig6 is required for DNA-damage-induced G2/M cell cycle arrest
- Mig6 binds to and stabilizes the Wee1 kinase by hindering the recruitment of βTrCP

Sasaki et al., 2018, Cell Reports *24*, 1278–1289
July 31, 2018 
https://doi.org/10.1016/j.celrep.2018.06.064

CellPress

OPEN ACCESS
CellPress

Cell Reports
Article

# The Tumor Suppressor MIG6 Controls Mitotic Progression and the G2/M DNA Damage Checkpoint by Stabilizing the WEE1 Kinase

Mari Sasaki,[1] Takeshi Terabayashi,[1,2] Stefanie M. Weiss,[1,3] and Ingvar Ferby[1,4,*]
[1]Department of Medical Biochemistry and Microbiology, Science for Life Laboratory, Uppsala University, Box 582, 751 23 Uppsala, Sweden
[2]Present address: Department of Pharmacology, Faculty of Medicine, Oita University, 1-1 Idaigaoka, Hasamamachi, 879-5593 Oita, Japan
[3]Present address: Toplab Gesellschaft für angewandte Biotechnologie mbH, Fraunhoferstr 18a, 82152 Martinsried, Germany
[4]Lead Contact
*Correspondence: ingvar.ferby@imbim.uu.se
https://doi.org/10.1016/j.celrep.2018.06.064

## SUMMARY

**MIG6 is an important tumor suppressor that binds to and negatively regulates epidermal growth factor receptor (EGFR). Here, we report an EGFR-independent function for MIG6 as an integral component of the cell cycle machinery. We found that depletion of MIG6 causes accelerated entry into and delayed exit from mitosis. This is due to premature and prolonged activation of CDK1, a key regulator of mitotic progression at the G2/M and meta- and anaphase transitions. Furthermore, MIG6 is required for inhibition of CDK1 upon DNA damage and subsequent G2/M cell cycle arrest. Mechanistically, we found that MIG6 depletion results in reduced phosphorylation of CDK1 on the inhibitory WEE1-targeted tyrosine-15 residue. MIG6 interacts with WEE1 and promotes its stability by interfering with the recruitment of the βTrCP-SCF E3 ubiquitin ligase and consequent proteasomal degradation of WEE1. Our findings uncover a critical role of MIG6 in cell cycle progression that is likely to contribute to its potent tumor-suppressive properties.**

## INTRODUCTION

Uncontrolled cell proliferation is a characteristic of cancer cells typically caused by excessive mitogenic signaling through growth factor receptors, such as epidermal growth factor receptor (EGFR), platelet-derived growth factor receptor (PDGFR), and c-MET in combination with loss of negative regulators of cell cycle progression (e.g., p53, RB, and p21). Negative constraint on the activity of EGFR and its family member ERBB2 is imposed by the multi-adaptor protein MIG6 (also called RALT or gene33 and encoded by the *ERRFI1* gene) that acts both by binding to and breaking up the activating kinase domain dimer (Anastasi et al., 2007; Ferby et al., 2006; Frosi et al., 2010; Hackel et al., 2001; Zhang et al., 2007a) and by targeting the receptors for degradation (Frosi et al., 2010; Ying et al., 2010). MIG6 has recently emerged as an important tumor suppressor. Loss of *MIG6* is frequent in cancer, and gene targeting of *MIG6* in mice disrupts epithelial homeostasis and causes spontaneous tumor formation in multiple organs (Ferby et al., 2006; Kim et al., 2013; Maity et al., 2015; Park et al., 2015; Reschke et al., 2010; Zhang et al., 2007b). It is unlikely that the highly potent tumor-suppressive activity of MIG6 can be solely attributed to its ability to restrain EGFR activity.

Many tumor suppressors negatively regulate cell cycle progression. Cyclin-dependent kinase (CDK)1 bound to its activator cyclin B is a key regulator of progression through mitosis. CDK1 activation drives entry into mitosis (Nurse, 1990), and inactivation drives exit from mitosis (Murray et al., 1989). CDK1 is inhibited by phosphorylation at tyrosine-15 and threonine-14 by the WEE1 and MYT1 kinases (Kornbluth et al., 1994; Mueller et al., 1995; Parker and Piwnica-Worms, 1992), and CDC25 phosphatases are responsible for de-phosphorylating these residues. Both inactivation of WEE1 and activation of CDC25 are necessary to trigger transition from G2 into M phase. CDK1 itself further phosphorylates and inactivates WEE1 and MYT1 and activates CDC25 in a feedback loop that results in a switch-like activation of CDK1 (O'Farrell, 2001). However, what normally keeps WEE1 active and CDC25 inactive during the S and G2 phases and what reverses their activities at the end of G2 remains poorly understood. The CDC25-WEE1-CDK1 system is also targeted in response to DNA damage, whereby phosphorylation of CDC25 and WEE1 by CHK1/CHK2 downstream of ATM/ATR is crucial for arresting cells in G2 to allow for repair of damaged DNA (Karlsson-Rosenthal and Millar, 2006; O'Connell et al., 1997; Raleigh and O'Connell, 2000).

Exit from mitosis requires CDK1 to be switched off, which is primarily accomplished by degradation of cyclin B during the metaphase to anaphase transition. In addition, CDK1 is inhibited by re-phosphorylation by WEE1 (D'Angiolella et al., 2007; Potapova et al., 2009, 2011) prior to full degradation of the cyclins. The importance of WEE1 re-activation during mitotic exit is not entirely clear; however, depletion of WEE1 delays mitotic exit, indicating that both mechanisms, namely cyclin degradation and WEE1 activation, contribute to turning off CDK1 at the end of mitosis. Moreover, regulated control of de-phosphorylation of CDK1 substrates by phosphatases, such as PP2 and PP1, is crucial for entry into and exit from mitosis (Hégarat et al., 2014; Mochida et al., 2009, 2010; Wu et al., 2009).

We here report that, besides its well-established role as a negative regulator of EGFR signaling, MIG6 controls mitotic

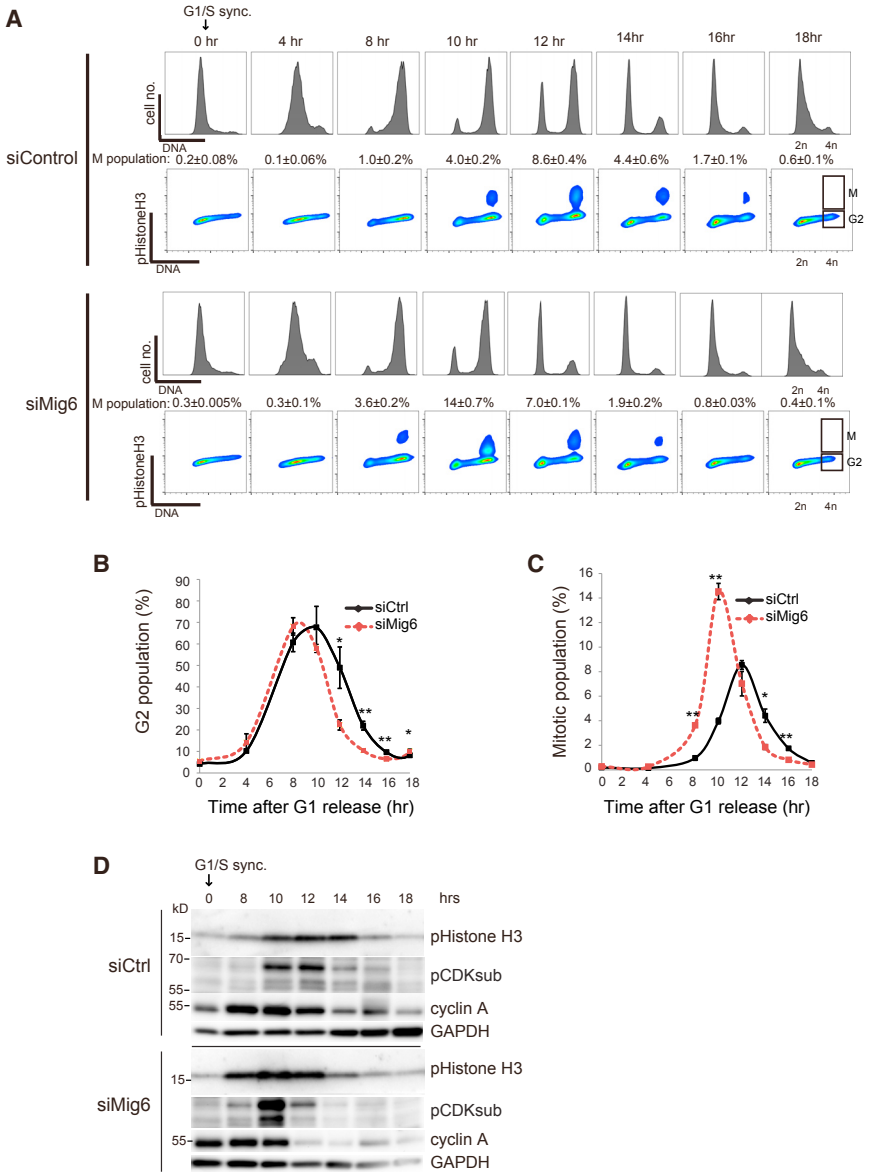


**Figure 1. MIG6 Depletion Causes Accelerated Entry into Mitosis**

(A) Flow cytometry analysis of control or *MIG6* siRNA-treated U2OS cells at indicated time points after release from synchronization at G1/S (double thymidine block). Panels on first and third rows show DNA profiles and second and fourth row phosphorylation of histone H3 on Ser-10 (pH3). Black boxes outline the gated G2 and mitotic cell populations.

(B and C) Quantification of cell cycle progression by flow cytometry of U2OS cells treated as in (A). Graphs show proportion of cells in G2 (B) or mitotic cells phosphorylated on histone H3 (C), gated as indicated in (A).

(D) Immunoblotting analysis of cell cycle markers of control or *MIG6* siRNA-treated U2OS cells at indicated time points after release from synchronization at G1/S (double thymidine block).

Data information: (A) representative of 3 independent experiments. In (B) and (C), data are presented as mean ± SD; n = 3. $^{**}p \leq 0.01$; $^{*}p \leq 0.05$ (two-tailed Student's t test).

progression through the unperturbed cell cycle. In addition, we find that MIG6 is required to sustain G2/M cell cycle arrest following DNA damage. We present evidence that this is due to the requirement of MIG6 to sustain WEE1 protein stability and subsequent inhibition of CDK1.

## RESULTS

### MIG6 Depletion Leads to Accelerated Entry into Mitosis

We and others have previously shown that *Mig6* knockout mice display severe defects in tissue development and homeostasis. Skin hyperplasia and increased skin tumor susceptibility caused by loss of *Mig6* was rescued by inhibition of Egfr (Ferby et al., 2006), which is consistent with a role of Mig6 as a negative regulator of EGFR. However, it is unlikely that the highly potent tumor-suppressive function of MIG6 can be solely attributed to its ability to negatively regulate EGFR signaling. We investigated whether MIG6, like other important tumor suppressors, plays a role in regulating the cell cycle. U2OS cells were synchronized at the G1/S border by double thymidine block followed by release from the block and assessment of cell cycle progression by flow cytometry with markers against DNA content (DAPI) or condensed chromatin (phospho-histone H3). We found that cells transfected with *MIG6* small interfering RNA (siRNA) progressed through the G2 phase (defined as 4N DNA: phospho-histone $H3^{-}$) approximately two hours faster than control siRNA-transfected cells (Figures 1A and 1B). Consequently, Mig6-depleted cells entered M phase (defined as phospho-histone $H3^{+}$) about two hours earlier than control cells (Figures 1A and 1C). The mitotic index of MIG6-depleted cells peaked at 10 hr after G1/S synchronization (mitotic index:14% ± 0.7%; dotted line Figure 1C), as compared with 12 hr in control treated cells (mitotic index: 8.6% ± 0.4% mitotic cells; full line Figure 1C). Furthermore, MIG6-depleted cells exited mitosis approximately one hour earlier than control cells (Figure 1C). Noticeably, we consistently observed higher peak mitotic index levels in MIG6-depleted as compared with control cells (Figure 1C; data not shown), which is consistent with transient accumulation of cells in mitosis.

To complement the flow cytometry data, we analyzed corresponding cell lysates by immunoblotting with selected cell cycle markers. In control cells, mitotic phosphorylation of histone H3 (pSer10) and CDK substrates (pTPxK) was evident 10 hr after release from G1/S in control siRNA-transfected cells, as compared with after 8 hr in *MIG6* siRNA-transfected cells

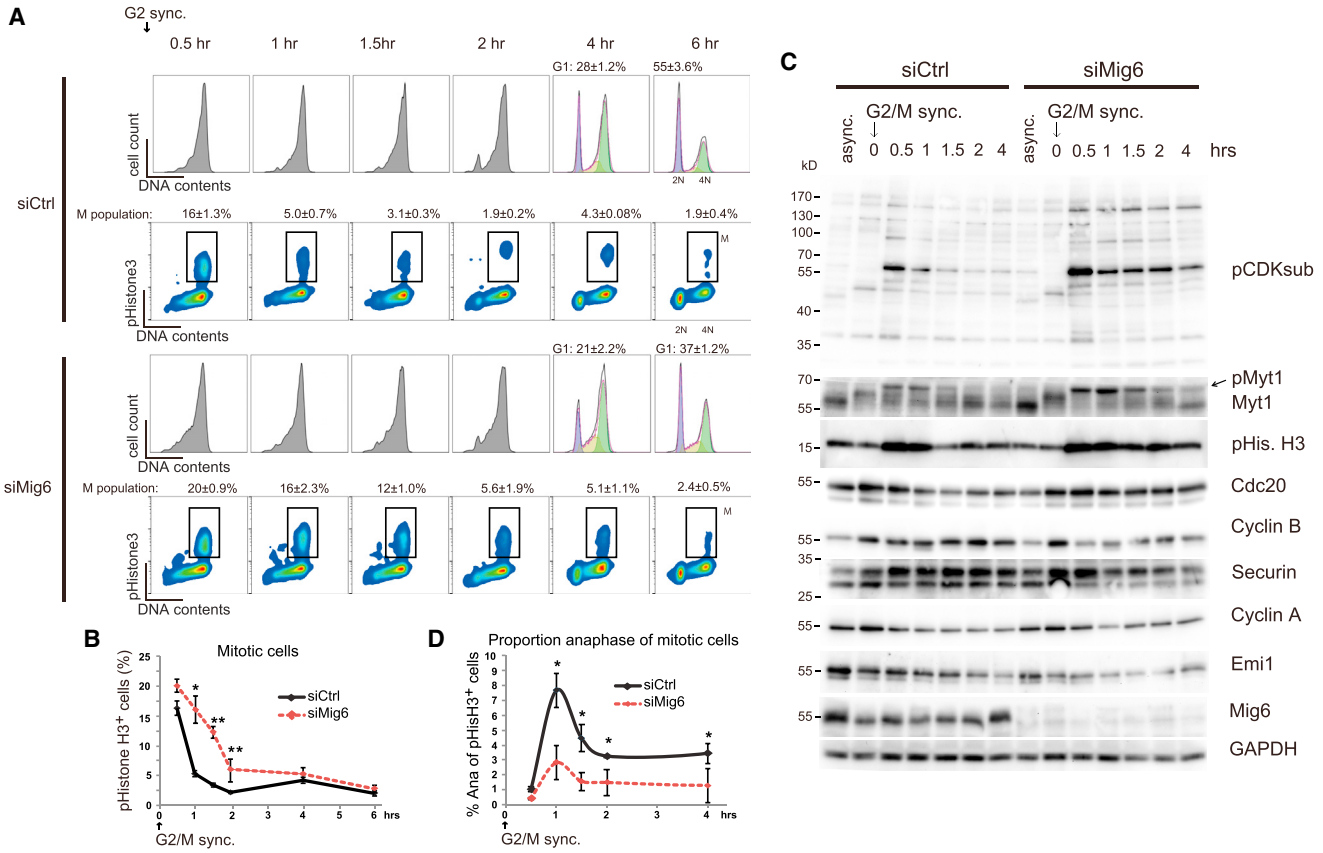


**Figure 2. MIG6 Depletion Causes Delayed Mitotic Exit**

(A) Flow cytometry analysis of control or *MIG6* siRNA-treated U2OS cells at indicated time points after release from synchronization at G2/M (17-hr treatment with 9 μM RO-3306). Panels on first and third rows show DNA profiles and second and fourth row show phosphorylation of histone H3 on Ser-10 (pH3). Black boxes outline the gated mitotic (M) cell populations.

(B) Quantification of the FACS data in (A) showing the proportion of phospho-histone H3-positive mitotic cells at indicated times after release from the G2 block.

(C) Western blot analysis of U2OS cells treated as in (A) with indicated cell cycle markers. Note that depletion of MIG6 causes increased phosphorylation of CDK1 substrates as indicated by blotting with a phospho-CDK motif (pTPXK) antibody or by band shift of the mitotic phospho-protein MYT1 and reduced levels of APC-CDC20-targeted proteins cyclin B and securin.

(D) Proportion of anaphase to total mitotic cells at indicated times after release from G2. Control or MIG6 siRNA-transfected cells were synchronized at G2/M with RO-3306 prior to release from the block for indicated times. Image-based flow cytometry was used to define the anaphase population according to experimental criteria outlined in Figure S2. The data are presented as proportion of anaphase cells out of all phospho-histone H3-positive cells. The lower proportion of anaphase cells of total mitotic cells in MIG6-depleted cells indicates prolonged pro- and metaphase.

Data information: (A, B, and D) data are presented as mean values ± SD; n = 3 independent experiments (A, B, and D). *p ≤ 0.05; **p ≤ 0.01 (two-tailed Student's t test). See also Figures S1–S3.

(Figure 1D). Furthermore, cyclin A degradation, which occurs mid-M phase, was evident two hours earlier in Mig6-depleted than in control cells after release from the G1/S block (Figure 1D). Taken together, these results show that loss of MIG6 leads to accelerated progression through the G2 phase and early entry into mitosis.

## Loss of MIG6 Causes Prolonged Activation of CDK1 during Mitosis and Delayed Mitotic Exit

To directly investigate the role of MIG6 in initiation of and transition through mitosis, we synchronized U2OS cells at the G2/M border of the cell cycle by 17-hr treatment with the reversible CDK1 inhibitor RO-3306 (Vassilev et al., 2006). Upon removal of RO-3306, the cells progressed through mitosis in a synchronized manner as monitored by flow cytometry (Figure 2A). By 6 hr, 55% ± 3.6% of U2OS cells transfected with control siRNA had undergone cell division and returned to the G1 phase, compared with only 37% ± 1.2% of cells transfected with *MIG6* siRNA (Figure 2A). Quantification of phospho-histone $H3^+$ cells revealed an approximately one-hour delay in mitotic exit in MIG6-depleted cells (Figure 2B). To gain better insight into the impact of MIG6 depletion on mitotic progression, we analyzed cells after release from the RO-3306 block by immunoblotting with selected cell cycle markers. Strikingly, depletion of MIG6 resulted in robust and prolonged activation of CDK1 as indicated by immunoblotting against phospho-CDK substrates (Figure 2C, upper panel) or by the appearance of a lower mobility form of MYT1, known to be hyper-phosphorylated in mitosis in

part by CDK1 (Booher et al., 1997; Ruiz et al., 2008; Wells et al., 1999; Mueller et al., 1995; Figure 2C, middle panel, arrow). Similar results were obtained using another independent siRNA (Figure S1A).

It has previously been reported that prolonged RO-3306 treatment leads to re-activation of anaphase promoting complex (APC); degradation of mitotic proteins, including CDC20; reduced phosphorylation of CDK1 on tyrosine-15; and consequently premature progression through mitosis and subsequent appearance of bi-nucleated cells (Prosser et al., 2012). However, such effects are unlikely to influence our experiments significantly because, although 22- and 38-hr treatments with RO-3306 caused some reduction of CDC20 levels or CDK tyrosine-15 phosphorylation, no noticeable effects were observed after 17 hr of treatment, which corresponds to the time span we used (Figure S1B). Nor did we observe appearance of bi-nucleated cells in the cell cycle profiles obtained by flow cytometry (Figure 2A).

Inactivation of CDK1 is required for mitotic exit and occurs in part through activation of the APC-CDC20 E3 ubiquitin ligase, which targets cyclin B for proteasomal degradation, and in part via inhibitory phosphorylation of CDK1 by WEE1. Once APC-CDC20 is active, CDK1/cyclinB is inactivated, which in turn targets CDC20 for degradation by APC-CDH1. This is because CDK1-mediated phosphorylation of CDH1 prevents it from binding APC (reviewed in Castro et al., 2005). We found that silencing of MIG6 delayed degradation of CDC20 during mitotic progression, which coincided with enhanced degradation of cyclin B and securin, which are known targets of APC-CDC20 (Figure 2C). This is presumably due to sustained CDK1-mediated phosphorylation of CDH1. Degradation of cyclin A, which occurs prior to degradation of cyclin B in mid-M phase, is unaffected by depletion of MIG6 (Figure 2C). These results suggest a role for MIG6 in limiting CDK1 activity during mitosis, through a mechanism other than inhibition of APC-mediated degradation of cyclin B.

## Loss of MIG6 Delays Progression through Metaphase

In order to better define the role of MIG6 during mitotic progression, we utilized fluorescence-imaging-based flow cytometry that enables resolving the distribution of cell populations in pro- and metaphase and anaphase while simultaneously assessing the activity of CDK1 with the pTPxK phospho-substrate antibody. Experimental parameters, including aspect ratio (nuclear shape), cell shape thresholding, phospho-histone H3, and phospho-CDK substrate detection, were optimized and validated as described in Figure S2A. U2OS cells transfected with control or *MIG6* siRNA were synchronized at G2/M, and their progression through mitosis was analyzed. MIG6-depleted cells exhibited a lower proportion of anaphase cells out of all mitotic (phospho-histone $H3^{+}$) cells over a 4-hr time span after release from the G2/M block, as compared with control-treated cells (Figure 2D). This is consistent with loss of MIG6 resulting in prolonged pro- and metaphase rather than prolonged anaphase. The metaphase to anaphase transition coincides with inactivation of CDK1. To test whether CDK activity remains elevated in anaphase in the absence of MIG6, we quantified the phospho-CDK1 substrate immunoreactivity specifically in the anaphase cell population 2 or 3 hr after release from the G2/M block, as determined by image-based flow cytometry (Figure S2B). We found that control or *MIG6* siRNA-transfected anaphase cells exhibited equal levels of CDK1 activity, suggesting that elevated residual CDK1 activity in anaphase does not contribute to the delayed mitotic exit in the absence of MIG6.

## MIG6 Regulates Cell Cycle Progression Independently of Its Role as a Negative Regulator of the ERBB Receptors

Given the well-established role of MIG6 as a negative regulator of the EGFR and ERBB2, it is possible that increased EGFR/ERBB2 signaling could underlie the effect of MIG6 loss on CDK1 activity. We therefore addressed whether pharmacological inhibition of EGFR/ERBB2 with the dual specificity antagonist lapatinib reverts the sustained mitotic activation of CDK1 observed in MIG6-depleted cells. U2OS cells were transfected with control or *MIG6* siRNA prior to G2 synchronization with RO-3306 and release from the block for 2 or 6 hr. At 2 hr post-release, high CDK1 activity was sustained in MIG6-depleted, but not control-treated, cells, as determined by immunoblotting against phospho-CDK substrates (Figure S3, upper panel) or the appearance of the upshifted CDK1-phosphorylated form of MYT1 (Figure S3, middle panel, arrow). Lapatinib treatment did not suppress the elevated CDK1 activity in MIG6-depleted cells, suggesting that MIG6 limits CDK1 activity independently of its role as a negative regulator of EGFR/ERBB2.

## MIG6 Promotes the Inhibitory Phosphorylation of CDK1 by WEE1

CDK1 activity is controlled by auto-amplifying positive feedback regulation, whereby its direct upstream regulators, CDC25 and WEE1 and MYT1, are themselves regulated by CDK1 phosphorylation. Therefore, to address whether Mig6 is an upstream regulator of CDK1 activity, we examined whether loss of Mig6 alters the regulatory status of CDK1 in cells arrested at the G2/M phase border with the CDK1 inhibitor RO-3306. Under these conditions, CDK1-mediated feedforward signaling is eliminated, thus facilitating interpretation of the results. We found that depletion of MIG6 led to 48% ± 9% (n = 7) reduction in phosphorylation levels of CDK1 at the inhibitory tyrosine-15 residue (Figures 3A and 3B). This reduction coincided with a comparable decrease in WEE1 protein levels (49% ± 18%; Figures 3A and 3B), although the levels of CDC25B and MYT1 were unaffected (Figure 3A). The observed decrease in WEE1 levels and tyrosine-15 phosphorylation of CDK1 was constant as cells progressed through mitosis after release from the G2 arrest (Figure 3C). Similarly, WEE1 levels were lower in MIG6-depleted cells synchronized at G1/S by double thymidine block at examined time points after release from the G1/S arrest (Figure 3D). We conclude that MIG6 is required for maintenance of WEE1 levels and subsequently effective phosphorylation of CDK1 at tyrosine-15.

## MIG6 Promotes WEE1 Stability

In order to test whether MIG6 controls WEE1 turnover, U2OS cells were either transfected with control or MIG6 siRNA followed by treatment with the protein synthesis inhibitor cycloheximide for increasing times. The levels of WEE1 were determined by immunoblotting (Figures 4A and 4B). WEE1 half-life decreased

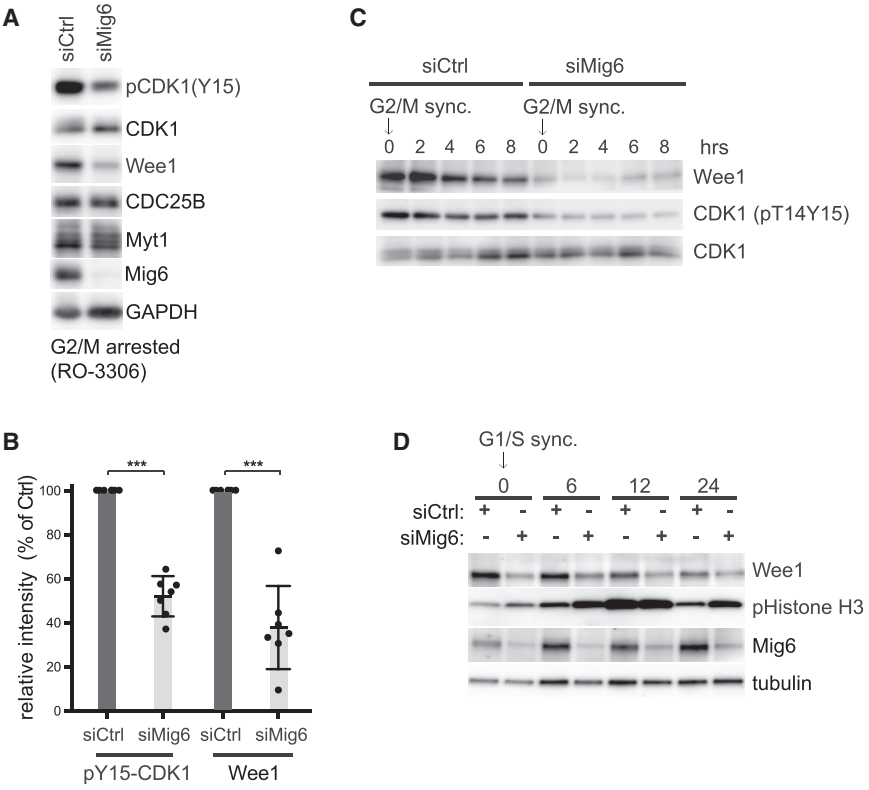


**Figure 3. MIG6 Promotes Inhibitory Phosphorylation of CDK1 on Tyrosine-15 by Preventing Proteasomal Degradation of WEE1**

(A) Immunoblotting of U2OS cells transfected with control (siCtrl) or *MIG6* siRNA (siMig6) prior to arrest at G2/M by treatment with 9 μM of the CDK inhibitor RO-3306 for 18 hr.

(B) Quantification of pCDK1(Y15) and WEE1 levels in U2OS cells treated with control (siCtrl) or *MIG6* siRNA (siMig6) prior to arrest at G2/M as described in (A). Values show band intensities of MIG6-depleted samples relative to control.

(C) Immunoblotting of control or *MIG6* siRNA-treated U2OS cells at indicated times after release from RO-3306-induced synchronization at G2/M. The data show reduced levels of WEE1 and reduced inhibitory phosphorylation of CDK1 on tyrosine-15 and threonine-14 in the absence of MIG6 during progression through mitosis.

(D) Immunoblotting against WEE1 and phosphohistone H3 of control or MIG6 siRNA-treated U2OS cells at indicated times following release from a double thymidine block (G1/S). Note that WEE1 levels are reduced upon loss of MIG6 all through the cell cycle.

Data information: (B) data presented as mean relative intensity ± SD (n = 7). ***$p \leq 0.001$ (one-sample Student's t test).

from about 6 hr in control cells to 3 hr in MIG6-depleted cells. WEE1 half-life was also reduced, although more modestly, in MIG6-depleted cells arrested at G1/S by thymidine block (Figures 4C and 4D).

We next asked whether MIG6 antagonizes proteasomal degradation of WEE1. U2OS cells were transfected with either control or *MIG6* siRNA prior to arrest at G2/M by 16-hr treatment with the CDK inhibitor and subsequent incubation with the proteasome inhibitor MG132 for 6 hr. Blocking the proteasome fully restored WEE1 protein levels (Figures 4E and 4F) and phosphorylation of CDK1 at tyrosine-15 (Figures 4E and 4G) in MIG6-depleted cells, suggesting that MIG6 regulates CDK1 activity by protecting WEE1 from proteasomal degradation. Regulation of turnover of many kinases involves negative feedback signaling or auto-phosphorylation. To address whether altered WEE1 kinase activity could play a part in regulating WEE1 stability in the absence of Mig6, U2OS cells were transfected with control or *MIG6* siRNA, followed by G2 synchronization with RO-3306 and the combined treatment with the WEE1 kinase inhibitor MK-1775 or vehicle for 18 hr (Figure 4H). MK-1775 treatment did not influence WEE1 levels in control or MIG6-depleted cells, suggesting that alteration in WEE1 activity does not regulate WEE1 stability in the presence or absence of MIG6 (Figure 4H).

## MIG6 Inhibits βTrCP-Dependent Ubiquitination of WEE1

Regulation of WEE1 turnover was found to depend on the SCF-βTrCP or SCF-Tome-1 E3 ubiquitin ligases (Watanabe et al., 2004, 2005; Smith et al., 2007). To test whether MIG6 regulates WEE1 stability at the level of ubiquitination, we transfected U2OS cells with control or *MIG6* siRNA, followed by transfection of myc-tagged WEE1 and hemagglutinin (HA)-ubiquitin. WEE1 was subsequently immunoprecipitated from isolated cell lysates and immunoblotted for HA-ubiquitin (Figure 5A). We found that ubiquitination of WEE1 was indeed substantially higher in MIG6-depleted cells. Notably, the experiment was conducted in the presence of MG132; hence, increased ubiquitination did not yield lower protein levels.

We next sought to determine which E3 ligase is responsible for increased ubiquitination of WEE1 in the absence of MIG6. U2OS cells were transfected with HA-ubiquitin and control or *MIG6* siRNA along with siRNA targeting either *βTrCP1/2*, *TOME-1*, or *CDC20*. WEE1 was then immunoprecipitated and blotted for HA-ubiquitin. The efficiency of depletion of CDC20, TrCP1/2, and MIG6 was validated by western blotting (Figure 5B). We were not able to detect endogenous TOME-1 in U2OS cells but could validate the efficiency of the siRNA on ectopically expressed TOME-1 (Figure S4A) or in HEK293T cells that express high levels of TOME-1 (Figure S4B). Depletion of βTrCP or TOME-1, but not CDC20, suppressed MIG6-loss-induced WEE1 ubiquitination to near basal levels (Figure 5B). This result suggests that MIG6 inhibits βTrCP1/2- and TOME-1-dependent ubiquitination of WEE1. To address whether WEE1 interacts with βTrCP1, βTrCP2, or TOME-1, we co-overexpressed myc-tagged WEE1 and flag-tagged βTrCP1, βTrCP2, or TOME-1. The F-box proteins were then immunoprecipitated and co-precipitating

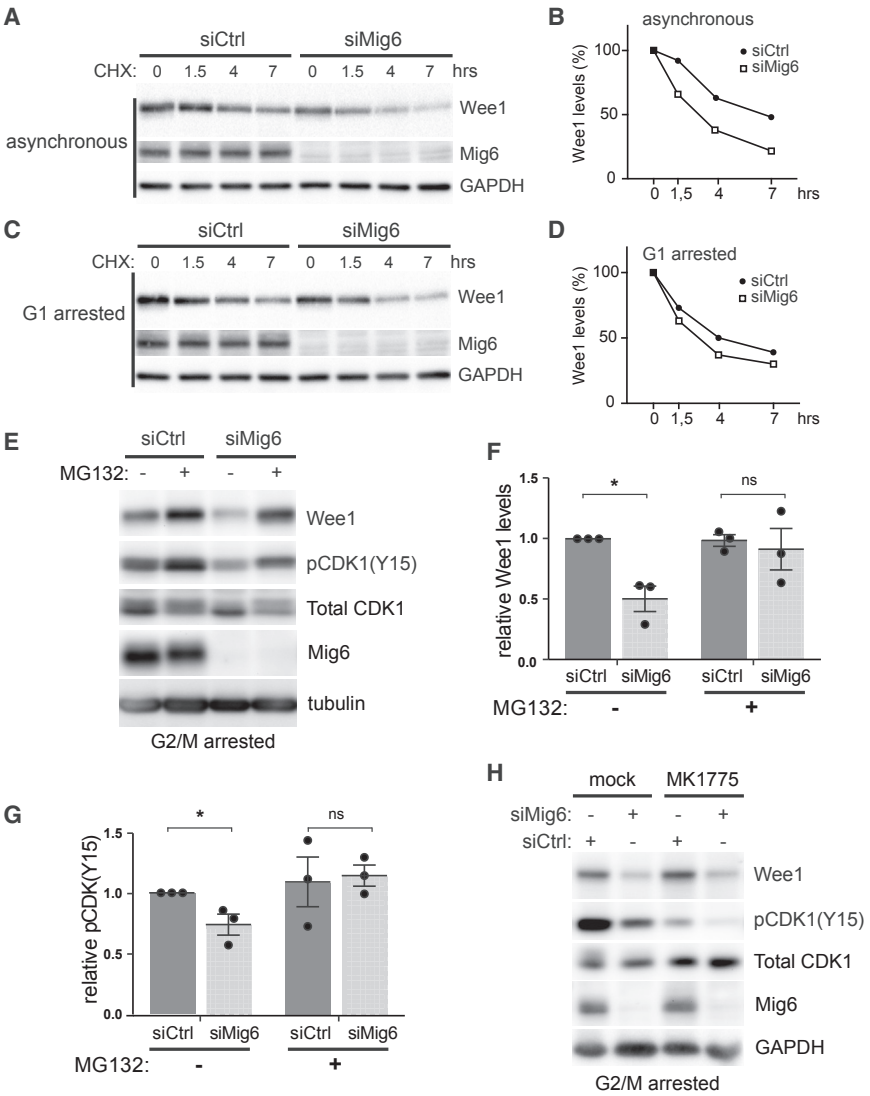


**Figure 4. MIG6 Promotes WEE1 Stability**

(A and B) Immunoblotting of U2OS cells transfected with control or MIG6 siRNA prior to treatment with the protein synthesis inhibitor cycloheximide for indicated times (A). Band intensity relative to untreated (0 hr) samples are quantified in (B).

(C and D) Immunoblotting of control or MIG6-depleted cells arrested at G1/S by double-thymidine block and treated with cycloheximide for indicated times (C). Band intensity relative to untreated (0 hr) samples are quantified in (D).

(E) Combined MIG6 depletion and inhibition of the proteasome. Immunoblotting of U2OS cells transfected with either control of MIG6 siRNA prior to cell cycle arrest at G2/M by treatment with RO-3306 for 24 hr is shown. During the last 6 hr, cells were additionally treated with the proteasome inhibitor MG132 (10 μM) or vehicle alone. Note that inhibition of the proteasome restores WEE1 protein levels and CDK phosphorylation on tyrosine-15 in MIG6-depleted cells.

(F and G) Quantification of relative mean band intensity of WEE1 (F) and pCDK1(Y15) (G) from 3 independent experiments conducted as in (E).

(H) Combined MIG6 depletion and inhibition of WEE1 activity. Immunoblotting of U2OS cells transfected with either control of MIG6 siRNA prior to cell cycle arrest at G2/M by treatment with RO-3306 for 24 hr together with the WEE1 inhibitor MK-1775 or vehicle (mock) is shown.

Data information: (F and G) data presented as mean relative intensity ± SD; n = 3 independent experiments; *p ≤ 0.05 (one-sample Student's t test). ns, non-significant.

## The Proline-Rich Region of MIG6 Interacts with the Kinase Domain of WEE1

Given that MIG6 interferes with the binding of βTrCP to WEE1, we addressed whether MIG6 interacts with WEE1. Ectopically expressed myc-WEE1 and flag-MIG6 co-immunoprecipitated efficiently in U2OS cells (Figure 6A). Furthermore, endogenous WEE1 co-immunoprecipitated with ectopically expressed MIG6 (Figure 6B). To determine whether the interaction between WEE1 and MIG6 is direct, we incubated recombinant glutathione S-transferase (GST)-tagged WEE1 with recombinant maltose-binding protein (MBP)-tagged MIG6 overnight and performed pull-down of GST and immunoblotting for bound MIG6 (Figure 6C). WEE1 and MIG6 co-precipitated efficiently *in vitro*, suggesting that the interaction is direct.

We next set out to map the regions of WEE1 and MIG6 involved in their interaction. Toward this end, we ectopically expressed tagged MIG6 along with wild-type or truncated forms of WEE1, lacking either the N-terminal domain or the C-terminal tail that contains the most prominent ubiquitination sites (source: PhosphositePlus database) or the kinase domain alone (Figures 6D and 6E). Flag-MIG6 immunoprecipitates were then analyzed for bound full-length or deleted WEE1 by immunoblotting. The data show that MIG6 binds to the kinase domain, but not the WEE1 assessed by immunoblotting (Figure S4C). WEE1 did not bind TOME-1 but effectively bound both βTrCP1 and -2. MIG6 overexpression partially reduced the WEE1-TrCP interaction (Figure 5C). TrCP has been reported to interact with the N-terminal regulatory domain of WEE1 (Watanabe et al., 2004, 2005) and in addition proposed to bind a second PEST motif within the kinase domain of WEE1 (Owens et al., 2010), although actual binding of βTrCP to the kinase domain remains to be demonstrated. We therefore tested whether the WEE1 kinase domain alone binds to TrCP1 and, if so, whether or not MIG6 interferes with the interaction. U2OS cells were co-transfected with a myc-tagged truncated form of WEE1 that contains only the kinase domain, along with Flag-TrCP1 and increasing amount of untagged MIG6. Flag-TrCP1 was then immunoprecipitated and bound WEE1 visualized by immunoblotting (Figure 5D). We found that the WEE1 kinase domain co-precipitated with TrCP1 in a manner that was gradually abolished by increasing expression of MIG6.

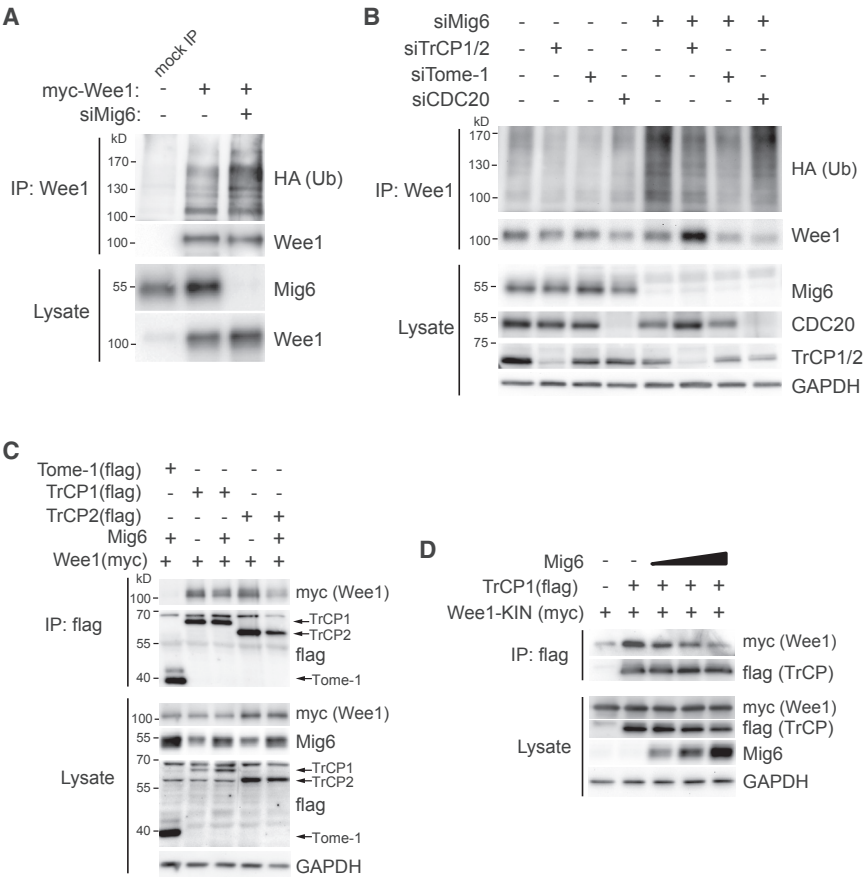


**Figure 5. MIG6 Interferes with βTrCP Recruitment and Ubiquitination of WEE1**

(A) Immunoprecipitation of myc-WEE1 co-expressed with HA-ubiquitin in U2OS cells transfected with control or *MIG6* siRNA followed by immunoblotting as indicated.

(B) Immunoprecipitation of endogenous WEE1 co-expressed with HA-ubiquitin in U2OS cells transfected with either control or MIG6 siRNA alone or together with TrCP1/2, TOME-1, or CDC20 siRNA, followed by immunoblotting as indicated. Note that depletion of TrCP1/2 or TOME-1 suppresses the elevated ubiquitination of WEE1 caused by depletion of MIG6.

(C) MIG6 overexpression interferes with binding of WEE1 to βTrCP1/2. Immunoprecipitation of myc-WEE1 co-expressed with βTrCP1, βTrCP2, or TOME-1, with or without MIG6, in U2OS cells and subsequent immunoblotting as indicated is shown.

(D) Co-immunoprecipitation of ectopically expressed myc-WEE1 with Flag-TrCP1, co-expressed with increasing amounts of MIG6. Cell lysates and immunoprecipitated were analyzed by immunoblotting as indicated.

See also Figure S4.

N-terminal domain or C-terminal tail, of WEE1 (Figure 6D). Conversely, we performed the equivalent experiments expressing full-length WEE1 with wild-type, truncated, or mutant forms of MIG6, including deletions of the N-terminal CRIB (CDC42-binding) domain, the ERBB-binding domain (EBR), the entire C-terminal half of the protein (N-term), or expressing the central proline-rich region alone (Pro-rich) (Figures 6F and 6G). MIG6 was immunoprecipitated (left panels: anti-MIG6; right panels: anti-Flag) and bound myc-WEE1 examined by immunoblotting (Figure 6F). WEE1 co-precipitated with all mutant MIG6 proteins, thus identifying the central proline-rich region of MIG6 as interacting with WEE1. Notably, we were unable to detect TrCP1 in the MIG6 immunoprecipitates, indicating that MIG6 and TrCP cannot bind WEE1 simultaneously (data not shown). Taken together, we conclude that MIG6 binds to the kinase domain of WEE1, and along with our previous observation that MIG6 interferes with the recruitment of TrCP1 to the WEE1 kinase domain (Figures 5C and 5D), we propose that MIG6 physically obstructs the recruitment of βTrCP to the WEE1 kinase domain, thereby preventing its proteasomal degradation.

## MIG6 Is Required for DNA-Damage-Induced G2/M Cell Cycle Arrest

CDK1 and its regulators WEE1 and CDC25 are crucial targets of DNA damage checkpoint signaling (Caspari and Hilditch, 2015; Raleigh and O'Connell, 2000; Saini et al., 2015). We therefore asked whether MIG6 also plays a role in inhibiting CDK1 in response to DNA damage. U2OS cells were transfected with control or MIG6 siRNA prior to synchronization at the G1/S border by double thymidine block and release followed by immediate 5 Gy ionizing radiation. The cells were subsequently analyzed by both flow cytometry (Figures 7A and 7B) and by immunoblotting against selected cell cycle marker (Figure 7C). Control-treated cells were predominantly arrested at G2 (58% ± 2%) 24 hr after irradiation, with only 21% ± 5% residing in G1 (Figure 7B). By contrast, at this point, MIG6-depleted cells had started to escape the arrest and divide with only 35% ± 0.2% of MIG6-depleted cells found in G2 and a significantly larger proportion of cells in G1 (37% ± 6%; Figures 7A and 7B). To complement the cell cycle profiling analysis, the equivalent samples were analyzed by immunoblotting against selected cell cycle markers. We found that 5 Gy irradiation of control siRNA-transfected cells resulted in accumulation of cyclin B and increased phosphorylation of CDK1 on tyrosine-15 in control siRNA-transfected cells 12 and 24 hr after irradiation (Figure 7C). By contrast, cyclin B levels and tyrosine-15 phosphorylation was significantly reduced in MIG6-depleted cells 24 hr after irradiation (Figure 7C), consistent with a requirement for MIG6 to sustain G2/M checkpoint arrest.

In order to further investigate the role of MIG6 for G2/M checkpoint signaling, we synchronized U2OS cells at the G2/M border with the CDK1 inhibitor RO-3306 and subjected them to 5 Gy gamma-irradiation prior to release from the cell cycle block and monitoring of cell cycle progression by DNA profiling and phospho-histone H3 immunostaining (Figure 7D). 4 hr post release, control siRNA-treated cells were arrested at the G2 phase (4N

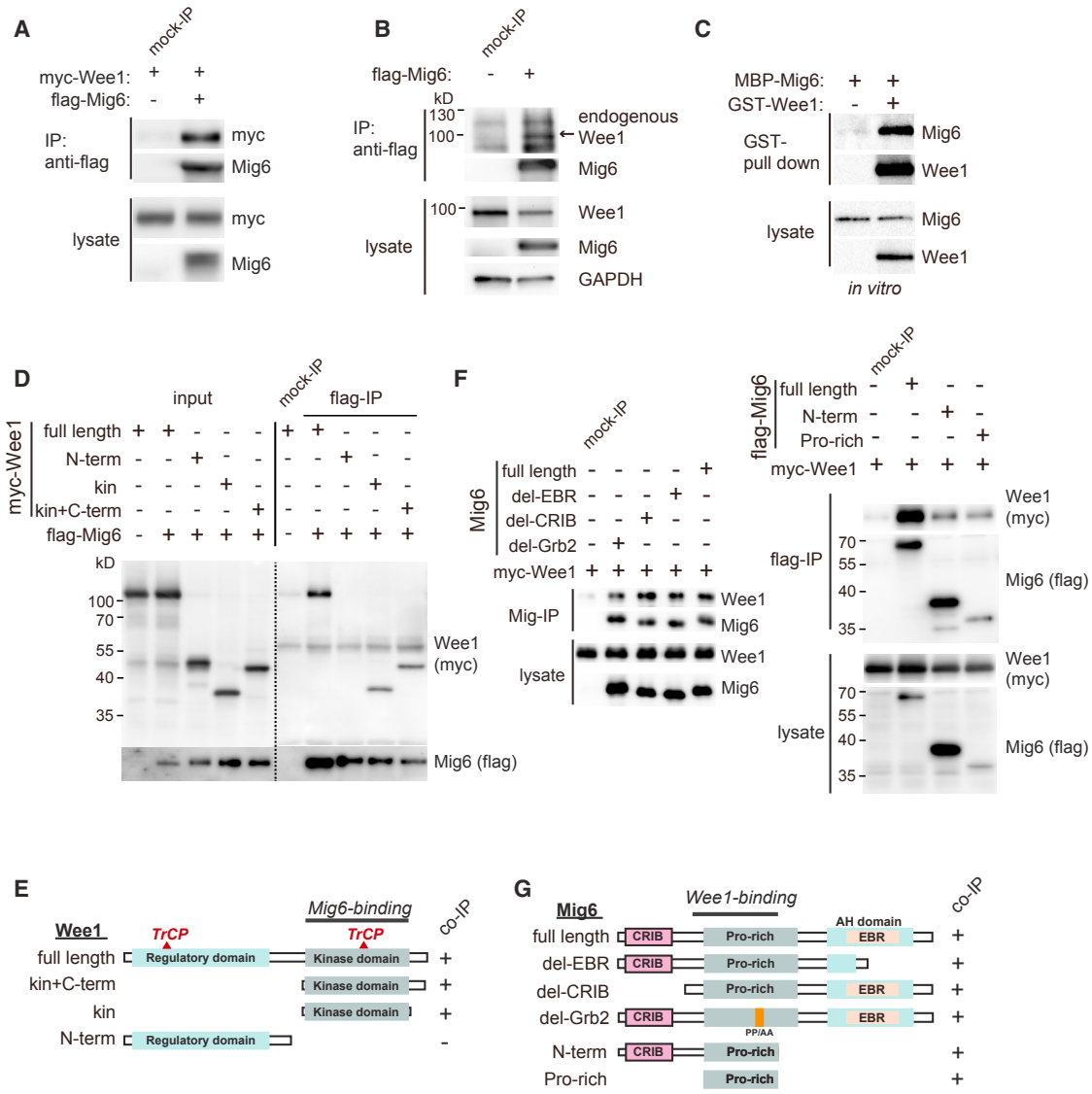


**Figure 6. MIG6 Directly Interacts with the Kinase Domain of WEE1**

(A) Co-immunoprecipitation of WEE1 and MIG6. U2OS cells were transfected with myc-WEE1 and Flag-MIG6 and arrested at G2/M by treatment with RO-3306, followed by anti-Flag immunoprecipitation (IP) and immunoblotting as indicated.

(B) Co-immunoprecipitation of endogenous WEE1 with Flag-MIG6 expressed in U2OS cells.

(C) GST-pull-down of recombinant WEE1 after overnight incubation with recombinant MBP-MIG6, followed by immunoblotting against MIG6 and WEE1.

(D and E) Co-immunoprecipitation of MIG6 with deletion mutants of WEE1. Flag-MIG6 was expressed in U2OS cells together with myc-tagged full-length WEE1; the N-terminal regulatory domain (N-term; aas 1–291); C-terminal half, including the kinase domain (kin+C-term; aas 292–end); or the kinase domain alone (kin; aas 292–575). Cell lysates were subjected to anti-Flag immunoprecipitation and immunoblotting against the myc (WEE1) (D). Note that all fragments except the N-term regulatory domain binds MIG6. The deletion mutant WEE1 proteins are schematically depicted in (E).

(F and G) Co-immunoprecipitation of WEE1 with mutant forms of MIG6. Myc-WEE1 was co-expressed with full-length MIG6 or mutant forms lacking the ERBB-receptor binding region (del-EBR; lacking aas 326–362), the CRIB domain (del-CRIB; lacking aas 1–42), or point mutant PP319/2AA with a disrupted GRB2 binding site (del-Grb2). Cell lysates were subjected to anti-MIG6 immunoprecipitation and immunoblotting against the WEE1 (F, left panels). Myc-WEE1 was co-expressed with Flag-tagged MIG6, the N-terminal half of MIG6 (N-term; aas 1–291), or the proline-rich central region (Pro-rich; aas 34–265). Flag-MIG6 was immunoprecipitated and bound WEE1 assessed by immunoblotting (F, right panels). The mutant MIG6 proteins are schematically depicted in (G).

DNA content; phospho-histone $H3^{-}$), although a significant proportion of MIG6-depleted cells had overcome the arrest and progressed into M phase (phospho-histone $H3^{+}$ cells) and G1 (2N DNA content; Figure 7D). It is possible that loss of MIG6 protects against damage inflicted to DNA by ionizing radiation or compromises the ability of cells to detect damage to the DNA. However, this does not appear to be the case because depletion of MIG6 did not alter phosphorylation of histone H2AX (Figure S5A), a marker of double-strand breaks, or phosphorylation of CHK2 on threonine-68 by the DNA-damage-sensing ATM/ATR kinases

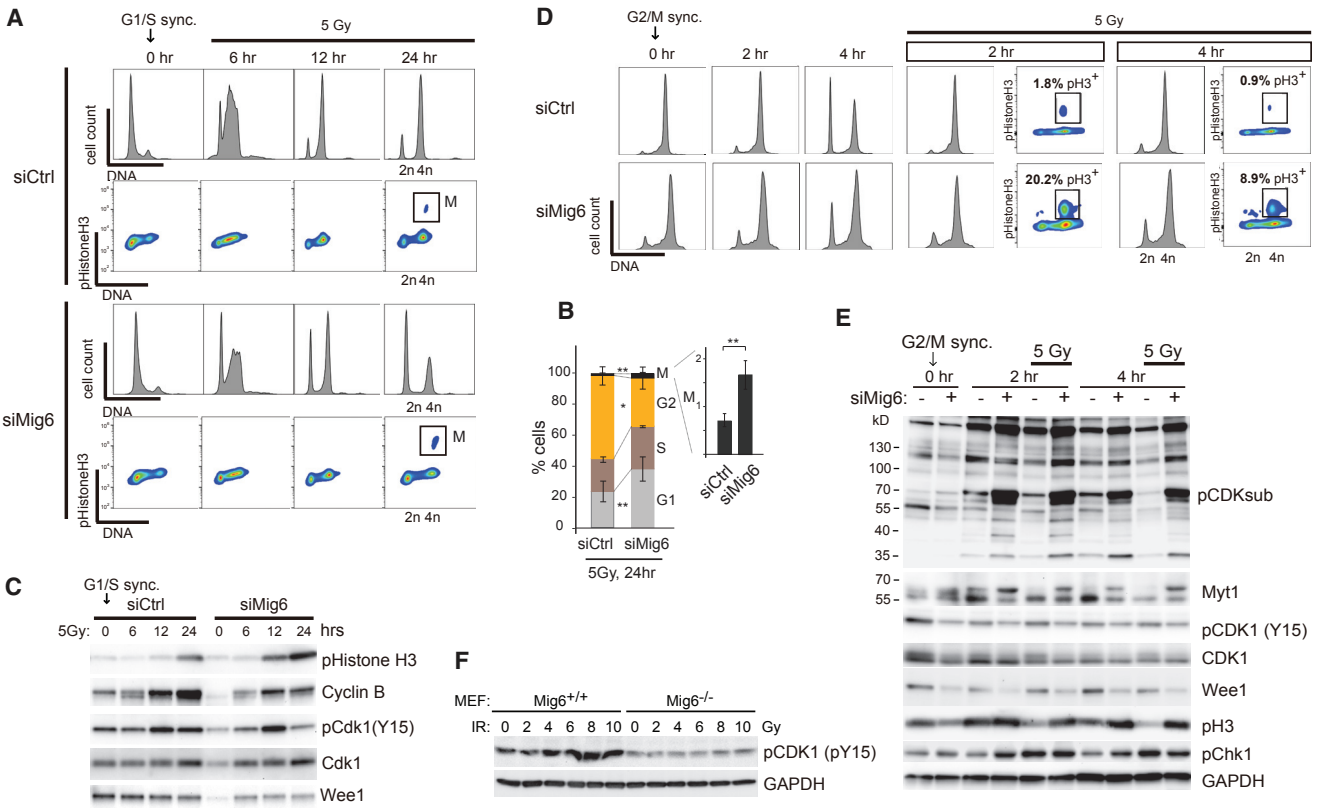


**Figure 7. MIG6 Is Required for DNA-Damage-Induced G2/M Cell Cycle Arrest**

(A) Flow cytometry analysis of control or MIG6 siRNA-treated U2OS cells at indicated time points after gamma radiation (5 Gy) and release from synchronization at G1/S (double-thymidine block). Upper panels show DNA profiles, and lower panels show phosphorylation of histone H3 (pH3).

(B) Quantification of cell cycle stages 24 hr after gamma irradiation of cells as described in (A).

(C) Immunoblot analysis of cells treated as in (A) with indicated cell cycle markers.

(D) Flow cytometry analysis of control or Mig6 siRNA-treated U2OS cells at indicated time points after gamma radiation (5 Gy) and release from synchronization with RO-3306 at G2/M. Note that Mig6 depletion leads to partial override of irradiation-induced G2/M cell cycle arrest.

(E) Immunoblotting of control or *MIG6* siRNA-transfected U2OS cells after block at G2/M with RO-3306, ionizing radiation, and subsequent release from the block for indicated times. Note that irradiation causes a reduction in CDK1 activity (pCDKsub and MYT1 upshift) in control cells, and CDK1 activity remained high in the absence of MIG6.

(F) Western blotting of wild-type or *Mig6*−/− mouse embryo fibroblasts (MEFs) one hour after gamma irradiation at increasing doses.

Data information: (B) data are presented as mean ± SD; n = 3 independent experiments. *p ≤ 0.05; **p ≤ 0.01 (two-tailed Student's t test). See also Figure S5.

(Figure S5B). These results are consistent with MIG6 playing a role in maintaining cell cycle arrest rather than initial sensing of DNA damage.

We next asked whether loss of MIG6 plays a role in regulating CDK1 activity in response to DNA damage, similar to its role during the unperturbed cell cycle. Cells arrested at the G2/M phase border were subjected to ionizing radiation followed by release from the cell cycle block. As expected, DNA damage triggered sustained suppression of CDK1 activity in wild-type cells, as evident by immunoblotting against phospho-CDK1 substrates or the mitotic CDK1 target MYT1 (Figure 7E). On the contrary, cells lacking MIG6 retained high levels of phosphorylation of CDK1 substrates, which correlated with reduced levels of both WEE1 protein and phosphorylation of CDK1 at tyrosine-15 (Figure 7E). Notably, DNA-damage-induced ATM/ATR-mediated phosphorylation of CHK1 (Figure 7E) or CHK2 (Figure S5B) at an early time points (2 and 1 hr post-irradiation, respectively) was not affected by loss of MIG6, consistent with a role of MIG6 upstream of WEE1 but downstream of ATM/ATR-mediated phosphorylation of CHK1/2 (Figure 7E). *Mig6* knockout mouse embryo fibroblasts also exhibited reduced phosphorylation of CDK1 on the inhibitory tyrosine-15 in response to DNA damage inflicted by increasing doses of ionizing radiation as compared to wild-type control (Figure 7F). We conclude that MIG6 is required to maintain G2/M cell cycle arrest in response to ionizing radiation likely by stabilizing WEE1 that in turn inhibits CDK1.

## DISCUSSION

Accumulating evidence support that MIG6 is a major tumor suppressor. However, the cellular function of this multi-adaptor protein is unlikely to be restricted to its established function as a negative feedback regulator of EGFR and ERBB2. In this study,

we have uncovered a function of MIG6 as a component of the cell cycle machinery that controls entry into and exit from mitosis, which may underlie its potent tumor-suppressive effects.

We have gained good understanding of how the master regulator of mitotic progression, CDK1, is inhibited in response to genotoxic stress, but we know less about what prevents CDK1 from becoming activated prematurely in the S/G2 phases of the unperturbed cell cycle. We found that loss of MIG6 leads to premature transition from G2 phase to mitosis as well as a delayed exit from mitosis. Our data reveal that MIG6 suppresses sustained CDK1 activation by promoting the phosphorylation of CDK1 on the inhibitory tyrosine-15 site. This provides a likely explanation for the role of MIG6 during mitotic progression because entry into mitosis depends on the activity of CDK1, and conversely, exit from mitosis requires that CDK1 is inactivated. Mechanistically, we show that MIG6 interacts with the WEE1 kinase domain and hinders the recruitment of TrCP and subsequent proteasomal degradation of WEE1. Previous work has shown that TrCP binding to the N-terminal regulatory region of WEE1 requires prior phosphorylation of WEE1 on Ser53 and Ser123 by PLK and CDK1, respectively (Watanabe et al., 2004). Our data show that MIG6 stabilizes WEE1 even under conditions when CDK1 is pharmacologically inactivated. This suggests that, contrary to the N-terminal binding site, TrCP binding to the WEE1 kinase domain, which is hindered by MIG6, does not require prior phosphorylation by CDK1. This may explain why MIG6 also stabilizes WEE1 in cells arrested at G1/S when CDK1 is inactive. Owens and colleagues (Owens et al., 2010) showed that TrCP targeting of WEE1 depends on three serines in the activation loop of the WEE1 kinase that likely needs to be phosphorylated in order for TrCP to dock. A plausible hypothesis would be that WEE1 itself auto-phosphorylates these sites; however, inhibition of WEE1 activity with MK-1775 did not attenuate the destabilization of WEE1 caused by MIG6 loss, indicating that a yet unidentified kinase is responsible for priming the kinase domain for recruitment of TrCP1.

Given the complex regulatory circuitry involving numerous kinases and phosphatases that regulate CDK1 activity and the mitotic transition, it should not be ruled out that MIG6 acts by additional means to regulate CDK1 activity and mitotic progression. However, in support of WEE1 being a primary cell cycle target of MIG6, loss of WEE1 similar to loss of MIG6 causes premature entry into mitosis and delayed mitotic exit (D'Angiolella et al., 2007; Potapova et al., 2009, 2011). In addition, WEE1 is targeted by the DNA damage checkpoint signaling and required to maintain inhibition of CDK1 during G2/M cell cycle arrest, similar to MIG6 (O'Connell et al., 1997; Raleigh and O'Connell, 2000). The identified role of MIG6 in G2/M checkpoint signaling is therefore also likely due to its ability to stabilize WEE1.

Premature entry into mitosis likely contributes to chromosomal instability (CIN) and carcinogenesis. Loss or downregulation of WEE1 has previously been linked to CIN in several cancer types, including colon cancer, prostate cancer, and non-small-cell lung cancer (NSCLC) (Backert et al., 1999; Kiviharju-af Hällström et al., 2007; Yoshida et al., 2004). Intriguingly, loss of *MIG6* occurs frequently in cancers, such as NSCLC; glioblastoma multiforme (GBM); and cancers of the breast, ovary, pancreas, and skin (Ferby et al., 2006; Li et al., 2012; Duncan et al., 2010; Ying et al., 2010). *Mig6* knockout mice are susceptible to formation of adenomas and adenocarcinomas in the lung, gastrointestinal tract, and skin (Ferby et al., 2006). It is therefore plausible that loss of MIG6 could cause CIN through downregulation of WEE1, thereby contributing to carcinogenesis.

In conclusion, we here uncover an unexpected role of MIG6 in controlling cell cycle progression and checkpoint response to DNA damage. In a broader context, these findings elevate MIG6 to the small family of important multifaceted tumor suppressors that function at multiple levels to restrain inappropriate cell proliferation. MIG6 may exert its tumor-suppressive functions by restricting mitogenic ERBB signaling (Ferby et al., 2006; Hackel et al., 2001; Anastasi et al., 2007); activating ABL to trigger cell death (Hopkins et al., 2012); and, as shown here, negatively regulating cell cycle progression through mitosis.

## EXPERIMENTAL PROCEDURES

### Plasmids and siRNA

*WEE1* was cloned into pcDNA3-myc vector, and *MIG6* was cloned into pCMVTag2B vector (FLAG-tagged MIG6), respectively. Mutant forms of mouse Mig6, delta-Grb2 (PP319/20AA), delta-CRIB (lacking amino acids [aas] 1–42), and delta-EBR (lacking aas 326–362), were cloned into pcDNA4/TO and mutated by site-directed mutagenesis, and N-term (aas 266–468) and Pro-rich (aas 34–265) were cloned into pCMVTag. *TrCP1*, *TrCP2*, and *TOME-1* cDNAs were kindly provided by Watanabe Nobumoto, Riken, Japan and sub-cloned into pCMVTag2B. Truncated forms of *WEE1*, kin+C-term (aas 292–end), kin (aas 292–575), and N-term (aas 1–291), were cloned into pcDNA3.1. The *MIG6* cDNA was sub-cloned into the pMALC2 vector for production of recombinant MBP-tagged MIG6 with amylose beads (New England Biolabs). The siRNA sequences against human *MIG6* were no. 1: 5′-GGAUAUCCAACUGUUGUAU-3′ and no. 2: 5′-GAACCUUUGUCACCGAGUA-3′ (Ambion). siRNA no. 1 was used unless otherwise stated. siRNA sequence against *TrCP1/2* is 5′-GGAAUUUGUGGAACAUCUU-3′. *CDC20*, *TOME-1*, and control siRNA was from Ambion s2748, s37945, and s4390847, respectively.

### Recombinant Proteins

Recombinant MBP-tagged MIG6 was expressed in BL21Star (DE3) bacterial strain and purified with amylose beads (New England Biolabs). Purified GST-tagged WEE1 was from Thermo Fisher Scientific.

### Antibodies

The following antibodies were used for western blotting: WEE1 (Santa Cruz Biotechnology sc5285); MIG6 (Sigma PE16); phospho-CDK1 (T14Y15; Thermo Fisher Scientific 710840); CDK1 (Santa Cruz sc54); phospho-CDK1 target (pTPXK; Cell Signaling Technology no. 14371); phospho-CDK1 (pY15; Cell Signal no. 9111); MYT1 (Cell Signal no. 4282); beta-TrCP (D13F10; Cell Signal no. 4394); securin (EPR3240; Abcam); EMI1 (3D2D6; Abcam); phospho-CHK1 (S345; Cell Signal no. 2348); phospho-CHK2 (T68; Cell Signal no. 2197); CHK2 (Abcam ab8108); gamma H2A.X-phospho S139; 9F3 (Abcam); CDC25B (Santa Cruz sc-326); cyclin B1 (Cell Signal no. 4138); cyclin A (Santa Cruz sc-271682); Flag (Sigma F7425); Myc (Abcam ab9132). Anti-phospho-histone 3 (S10) antibodies for fluorescence-activated cell sorting (FACS) and immunoblot analysis were from Thermo Scientific (MA5-15220) and Millipore (06-570), respectively.

### Cell Culture and Inhibitor Treatments

U2OS and HEK293T cells were cultured in DMEM supplemented with 10% fetal bovine serum at 37°C in 5% CO2. siRNAs and plasmid DNA were transfected using Lipofectamine RNAiMax and Lipofectamine 3000 (Invitrogen) according to manufacturer's instruction. Cell cycle synchronization at G1/S was achieved by double thymidine block (20.5 hr treatment with 2 mM thymidine [Sigma], followed by 7 hr of release and a second 16.5-hr block with

thymidine). Cell cycle synchronization at G1/S was achieved by treatment for 16–18 hr with 9 μM of RO-3306 (Calbiochem). Cells were treated with cycloheximide at a dose of 10 μg/mL or MG132 at 10 μM for indicated times.

### Image-Based Flow Cytometry

Cells were fixed with 70% ethanol and stained with mouse anti-phospho-histone H3 and rabbit anti-phosphoCDK1substrate followed by incubation with secondary antibodies anti-rabbit immunoglobulin G (IgG) AF546 and anti-mouse IgG AF647. After staining with DAPI, cells were analyzed on Flowsight imaging flow cytometer as described (Figure S2). Data were analyzed with the IDEAS and FlowJo software.

### Western Blot

Cells were lysed in 50 mM Tris (pH 8.0), 150 mM NaCl, 1% SDS, 0.5% sodium deoxycholate, 1% Triton X-100 with protease and phosphatase inhibitor cocktail (Thermo Scientific), 1 mM sodium orthovanadate, and Benzonase Nuclease added. Protein samples (10 μg per lane) were separated by SDS-PAGE electrophoresis and immunoblotted on polyvinylidene fluoride (PVDF) membranes and detection by ECL using a charge-coupled device (CCD) camera. Densitometric quantification was done using the ImageJ software. Wee1 expression levels and phospho-CDK1 levels were normalized against expression levels of either GAPDH or tubulin or total CDK1, respectively.

### Immunoprecipitation

U2OS cells were transfected with plasmids expressing myc-tagged WEE1 and FLAG-tagged MIG6. The cells were harvested in 50 mM Tris (pH 8.0), 150 mM NaCl, 1 mM EDTA, 0.5% NP40 with protease and phosphatase inhibitors (Thermo Fisher Scientific), and 1 mM sodium orthovanadate, after treatment with 9 μM RO-3306 for 17 hr followed by incubation with anti-FLAG beads (Sigma). Immunocomplexes were resolved by SDS-PAGE, and co-immunoprecipitated proteins were detected by immunoblotting.

### Irradiation

Cells were irradiated with $^{137}$Cs γ-ray photons (Gammacell 40 Exactor, MDS Nordion, Kanata, Canada) at a dose rate of ~1 Gy/min.

### Statistical Analyses

Two-tailed paired Student's t test was used to compare single parameters between two conditions, unless one condition was normalized to one, in which case one-sample Student's t test was used. Analysis was performed using GraphPad Prism 7.

## SUPPLEMENTAL INFORMATION

Supplemental Information includes five figures and can be found with this article online at https://doi.org/10.1016/j.celrep.2018.06.064.

## ACKNOWLEDGMENTS

The authors acknowledge the assistance of Noura Al-Walai and support of the BioVis Platform, Uppsala University with the FACS and Flowsight experiments. We thank Carl-Henrik Heldin and Taija Mäkinen for valuable discussion and Bo Stenerlöw for access and advice on the γ-ray irradiation source. This work was supported by the Ludwig Foundation, the Swedish Research Council (grant number: 2014-03445), and the Swedish Cancer Society (grant number: CAN 2015/752).

## AUTHOR CONTRIBUTIONS

M.S. and, to a limited extent, T.T. and S.M.W. designed and performed experiments and analyzed data. M.S. and I.F. wrote the manuscript. I.F. designed experiments and supervised the research.

## DECLARATION OF INTERESTS

The authors declare no competing interests.

Received: May 8, 2017
Revised: March 7, 2018
Accepted: June 13, 2018
Published: July 31, 2018

## REFERENCES

Anastasi, S., Baietti, M.F., Frosi, Y., Alemà, S., and Segatto, O. (2007). The evolutionarily conserved EBR module of RALT/MIG6 mediates suppression of the EGFR catalytic activity. Oncogene *26*, 7833–7846.

Backert, S., Gelos, M., Kobalz, U., Hanski, M.L., Böhm, C., Mann, B., Lövin, N., Gratchev, A., Mansmann, U., Moyer, M.P., et al. (1999). Differential gene expression in colon carcinoma cells and tissues detected with a cDNA array. Int. J. Cancer *82*, 868–874.

Booher, R.N., Holman, P.S., and Fattaey, A. (1997). Human Myt1 is a cell cycle-regulated kinase that inhibits Cdc2 but not Cdk2 activity. J. Biol. Chem. *272*, 22300–22306.

Caspari, T., and Hilditch, V. (2015). Two distinct Cdc2 pools regulate cell cycle progression and the DNA damage response in the fission yeast S.pombe. PLoS ONE *10*, e0130748.

Castro, A., Bernis, C., Vigneron, S., Labbé, J.-C., and Lorca, T. (2005). The anaphase-promoting complex: a key factor in the regulation of cell cycle. Oncogene *24*, 314–325.

D'Angiolella, V., Palazzo, L., Santarpia, C., Costanzo, V., and Grieco, D. (2007). Role for non-proteolytic control of M-phase-promoting factor activity at M-phase exit. PLoS ONE *2*, e247.

Duncan, C.G., Killela, P.J., Payne, C.A., Lampson, B., Chen, W.C., Liu, J., Solomon, D., Waldman, T., Towers, A.J., Gregory, S.G., et al. (2010). Integrated genomic analyses identify ERRFI1 and TACC3 as glioblastoma-targeted genes. Oncotarget *1*, 265–277.

Ferby, I., Reschke, M., Kudlacek, O., Knyazev, P., Pantè, G., Amann, K., Sommergruber, W., Kraut, N., Ullrich, A., Fässler, R., and Klein, R. (2006). Mig6 is a negative regulator of EGF receptor-mediated skin morphogenesis and tumor formation. Nat. Med. *12*, 568–573.

Frosi, Y., Anastasi, S., Ballarò, C., Varsano, G., Castellani, L., Maspero, E., Polo, S., Alemà, S., and Segatto, O. (2010). A two-tiered mechanism of EGFR inhibition by RALT/MIG6 via kinase suppression and receptor degradation. J. Cell Biol. *189*, 557–571.

Hackel, P.O., Gishizky, M., and Ullrich, A. (2001). Mig-6 is a negative regulator of the epidermal growth factor receptor signal. Biol. Chem. *382*, 1649–1662.

Hégarat, N., Vesely, C., Vinod, P.K., Ocasio, C., Peter, N., Gannon, J., Oliver, A.W., Novák, B., and Hochegger, H. (2014). PP2A/B55 and Fcp1 regulate Greatwall and Ensa dephosphorylation during mitotic exit. PLoS Genet. *10*, e1004004.

Hopkins, S., Linderoth, E., Hantschel, O., Suarez-Henriques, P., Pilia, G., Kendrick, H., Smalley, M.J., Superti-Furga, G., and Ferby, I. (2012). Mig6 is a sensor of EGF receptor inactivation that directly activates c-Abl to induce apoptosis during epithelial homeostasis. Dev. Cell *23*, 547–559.

Karlsson-Rosenthal, C., and Millar, J.B.A. (2006). Cdc25: mechanisms of checkpoint inhibition and recovery. Trends Cell Biol. *16*, 285–292.

Kim, T.H., Lee, D.-K., Cho, S.-N., Orvis, G.D., Behringer, R.R., Lydon, J.P., Ku, B.J., McCampbell, A.S., Broaddus, R.R., and Jeong, J.-W. (2013). Critical tumor suppressor function mediated by epithelial Mig-6 in endometrial cancer. Cancer Res. *73*, 5090–5099.

Kiviharju-af Hällström, T.M., Jäämaa, S., Mönkkönen, M., Peltonen, K., Andersson, L.C., Medema, R.H., Peehl, D.M., and Laiho, M. (2007). Human prostate epithelium lacks Wee1A-mediated DNA damage-induced checkpoint enforcement. Proc. Natl. Acad. Sci. USA *104*, 7211–7216.

Kornbluth, S., Sebastian, B., Hunter, T., and Newport, J. (1994). Membrane localization of the kinase which phosphorylates p34cdc2 on threonine 14. Mol. Biol. Cell *5*, 273–282.

Li, Z., Dong, Q., Wang, Y., Qu, L., Qiu, X., and Wang, E. (2012). Downregulation of Mig-6 in nonsmall-cell lung cancer is associated with EGFR signaling. Mol. Carcinog. *51*, 522–534.

Maity, T.K., Venugopalan, A., Linnoila, I., Cultraro, C.M., Giannakou, A., Nemati, R., Zhang, X., Webster, J.D., Ritt, D., Ghosal, S., et al. (2015). Loss of MIG6 accelerates initiation and progression of mutant epidermal growth factor receptor-driven lung adenocarcinoma. Cancer Discov. *5*, 534–549.

Mochida, S., Ikeo, S., Gannon, J., and Hunt, T. (2009). Regulated activity of PP2A-B55 delta is crucial for controlling entry into and exit from mitosis in Xenopus egg extracts. EMBO J. *28*, 2777–2785.

Mochida, S., Maslen, S.L., Skehel, M., and Hunt, T. (2010). Greatwall phosphorylates an inhibitor of protein phosphatase 2A that is essential for mitosis. Science *330*, 1670–1673.

Mueller, P.R., Coleman, T.R., Kumagai, A., and Dunphy, W.G. (1995). Myt1: a membrane-associated inhibitory kinase that phosphorylates Cdc2 on both threonine-14 and tyrosine-15. Science *270*, 86–90.

Murray, A.W., Solomon, M.J., and Kirschner, M.W. (1989). The role of cyclin synthesis and degradation in the control of maturation promoting factor activity. Nature *339*, 280–286.

Nurse, P. (1990). Universal control mechanism regulating onset of M-phase. Nature *344*, 503–508.

O'Connell, M.J., Raleigh, J.M., Verkade, H.M., and Nurse, P. (1997). Chk1 is a wee1 kinase in the G2 DNA damage checkpoint inhibiting cdc2 by Y15 phosphorylation. EMBO J. *16*, 545–554.

O'Farrell, P.H. (2001). Triggering the all-or-nothing switch into mitosis. Trends Cell Biol. *11*, 512–519.

Owens, L., Simanski, S., Squire, C., Smith, A., Cartzendafner, J., Cavett, V., Caldwell Busby, J., Sato, T., and Ayad, N.G. (2010). Activation domain-dependent degradation of somatic Wee1 kinase. J. Biol. Chem. *285*, 6761–6769.

Park, E., Kim, N., Ficarro, S.B., Zhang, Y., Lee, B.I., Cho, A., Kim, K., Park, A.K.J., Park, W.-Y., Murray, B., et al. (2015). Structure and mechanism of activity-based inhibition of the EGF receptor by Mig6. Nat. Struct. Mol. Biol. *22*, 703–711.

Parker, L.L., and Piwnica-Worms, H. (1992). Inactivation of the p34cdc2-cyclin B complex by the human WEE1 tyrosine kinase. Science *257*, 1955–1957.

Potapova, T.A., Daum, J.R., Byrd, K.S., and Gorbsky, G.J. (2009). Fine tuning the cell cycle: activation of the Cdk1 inhibitory phosphorylation pathway during mitotic exit. Mol. Biol. Cell *20*, 1737–1748.

Potapova, T.A., Sivakumar, S., Flynn, J.N., Li, R., and Gorbsky, G.J. (2011). Mitotic progression becomes irreversible in prometaphase and collapses when Wee1 and Cdc25 are inhibited. Mol. Biol. Cell *22*, 1191–1206.

Prosser, S.L., Samant, M.D., Baxter, J.E., Morrison, C.G., and Fry, A.M. (2012). Oscillation of APC/C activity during cell cycle arrest promotes centrosome amplification. J. Cell Sci. *125*, 5353–5368.

Raleigh, J.M., and O'Connell, M.J. (2000). The G(2) DNA damage checkpoint targets both Wee1 and Cdc25. J. Cell Sci. *113*, 1727–1736.

Reschke, M., Ferby, I., Stepniak, E., Seitzer, N., Horst, D., Wagner, E.F., and Ullrich, A. (2010). Mitogen-inducible gene-6 is a negative regulator of epidermal growth factor receptor signaling in hepatocytes and human hepatocellular carcinoma. Hepatology *51*, 1383–1390.

Ruiz, E.J., Hunt, T., and Nebreda, A.R. (2008). Meiotic inactivation of Xenopus Myt1 by CDK/XRINGO, but not CDK/cyclin, via site-specific phosphorylation. Mol. Cell *32*, 210–220.

Saini, P., Li, Y., and Dobbelstein, M. (2015). Wee1 is required to sustain ATR/Chk1 signaling upon replicative stress. Oncotarget *6*, 13072–13087.

Smith, A., Simanski, S., Fallahi, M., and Ayad, N.G. (2007). Redundant ubiquitin ligase activities regulate wee1 degradation and mitotic entry. Cell Cycle *6*, 2795–2799.

Vassilev, L.T., Tovar, C., Chen, S., Knezevic, D., Zhao, X., Sun, H., Heimbrook, D.C., and Chen, L. (2006). Selective small-molecule inhibitor reveals critical mitotic functions of human CDK1. Proc. Natl. Acad. Sci. USA *103*, 10660–10665.

Watanabe, N., Arai, H., Nishihara, Y., Taniguchi, M., Watanabe, N., Hunter, T., and Osada, H. (2004). M-phase kinases induce phospho-dependent ubiquitination of somatic Wee1 by SCFbeta-TrCP. Proc. Natl. Acad. Sci. USA *101*, 4419–4424.

Watanabe, N., Arai, H., Iwasaki, J., Shiina, M., Ogata, K., Hunter, T., and Osada, H. (2005). Cyclin-dependent kinase (CDK) phosphorylation destabilizes somatic Wee1 via multiple pathways. Proc. Natl. Acad. Sci. USA *102*, 11663–11668.

Wells, N.J., Watanabe, N., Tokusumi, T., Jiang, W., Verdecia, M.A., and Hunter, T. (1999). The C-terminal domain of the Cdc2 inhibitory kinase Myt1 interacts with Cdc2 complexes and is required for inhibition of G(2)/M progression. J. Cell Sci. *112*, 3361–3371.

Wu, J.Q., Guo, J.Y., Tang, W., Yang, C.-S., Freel, C.D., Chen, C., Nairn, A.C., and Kornbluth, S. (2009). PP1-mediated dephosphorylation of phosphoproteins at mitotic exit is controlled by inhibitor-1 and PP1 phosphorylation. Nat. Cell Biol. *11*, 644–651.

Ying, H., Zheng, H., Scott, K., Wiedemeyer, R., Yan, H., Lim, C., Huang, J., Dhakal, S., Ivanova, E., Xiao, Y., et al. (2010). Mig-6 controls EGFR trafficking and suppresses gliomagenesis. Proc. Natl. Acad. Sci. USA *107*, 6912–6917.

Yoshida, T., Tanaka, S., Mogi, A., Shitara, Y., and Kuwano, H. (2004). The clinical significance of cyclin B1 and Wee1 expression in non-small-cell lung cancer. Ann. Oncol. *15*, 252–256.

Zhang, X., Pickin, K.A., Bose, R., Jura, N., Cole, P.A., and Kuriyan, J. (2007a). Inhibition of the EGF receptor by binding of MIG6 to an activating kinase domain interface. Nature *450*, 741–744.

Zhang, Y.-W., Staal, B., Su, Y., Swiatek, P., Zhao, P., Cao, B., Resau, J., Sigler, R., Bronson, R., and Vande Woude, G.F. (2007b). Evidence that MIG-6 is a tumor-suppressor gene. Oncogene *26*, 269–276.